


# Finite element simulation of Love wave sensor for the detection of volatile organic gases

Yan Wang(王艳), Su-Peng Liang(梁苏鹏), Shu-Lin Shang(商树林),Yong-Bing Xiao(肖勇兵), and Yu-Xin Yuan(袁宇鑫)

**Citation:**Chin. Phys. B, 2022, 31 (**3**): 030701. DOI: 10.1088/1674-1056/ac3ec9
Journal homepage: http://cpb.iphy.ac.cn; http://iopscience.iop.org/cpb

**What follows is a list of articles you may be interested in**

---

## Effect of staggered array structure on the flow field of micro gas chromatographic column

Daohan Ge(葛道晗), Zhou Hu(胡州), Liqiang Zhang(张立强), and Shining Zhu(祝世宁)
Chin. Phys. B, 2022, 31 (**1**): 010701. DOI: 10.1088/1674-1056/ac0902

## A modified analytical model of the alkali-metal atomic magnetometer employing longitudinal carrier field

Chang Chen(陈畅), Yi Zhang(张燚), Zhi-Guo Wang(汪之国), Qi-Yuan Jiang(江奇渊), Hui Luo(罗晖), and Kai-Yong Yang(杨开勇)
Chin. Phys. B, 2021, 30 (**5**): 050707. DOI: 10.1088/1674-1056/abd7d3

## *In-situ* fabrication of ZnO nanoparticles sensors based on gas-sensing electrode for ppb-level $H_2S$ detection at room temperature

Jing-Yue Xuan(宣景悦), Guo-Dong Zhao(赵国栋), Xiao-Bo Shi(史小波), Wei Geng(耿伟), Heng-Zheng Li(李恒征), Mei-Ling Sun(孙美玲), Fu-Chao Jia(贾福超), Shu-Gang Tan(谭树刚), Guang-Chao Yin(尹广超), and Bo Liu(刘波)
Chin. Phys. B, 2021, 30 (**2**): 020701. DOI: 10.1088/1674-1056/abcf46

## Acetone sensors for non-invasive diagnosis of diabetes based on metal-oxide-semiconductor materials

Yujie Li(李育洁), Min Zhang(张敏), Haiming Zhang(张海明)
Chin. Phys. B, 2020, 29 (**9**): 090702. DOI: 10.1088/1674-1056/aba60b

## Room temperature $NO_2$-sensing properties of hexagonal tungsten oxide nanorods

Yaqiao Wu(武雅乔), Ming Hu(胡明), Yuming Tian(田玉明)
Chin. Phys. B, 2017, 26 (**2**): 020701. DOI: 10.1088/1674-1056/26/2/020701

---

# Finite element simulation of Love wave sensor for the detection of volatile organic gases

Yan Wang(王艳)†, Su-Peng Liang(梁苏鹏), Shu-Lin Shang(商树林), Yong-Bing Xiao(肖勇兵), and Yu-Xin Yuan(袁宇鑫)

*College of Electronic and Optical Engineering & College of Microelectronics, Nanjing University of Posts and Telecommunications, Nanjing* 210046, *China*

(Received 25 January 2021; revised manuscript received 13 October 2021; accepted manuscript online 1 December 2021)

The three-dimensional (3D) finite element (FE) simulation and analysis of Love wave sensors based on polyisobutylene (PIB) layers/$SiO_2$/ST-90°X quartz structure are presented in this paper, as well as the investigation of coupled resonance effect on the acoustic properties of the devices. The mass sensitivity of the basic Love wave device with $SiO_2$ guiding layers is solved analytically. And the highest mass sensitivity of 128 $m^2$/kg is obtained as $h_s/\lambda = 0.175$. The sensitivity of the Love wave sensors for sensing volatile organic compounds (VOCs) is greatly improved due to the presence of coupled resonance induced by the PIB nanorods on the device surface. The frequency shifts of the sensor corresponding to $CH_2Cl_2$, $CHCl_3$, $CCl_4$, $C_2Cl_4$, $CH_3Cl$ and $C_2HCl_3$ with the concentration of 100 ppm are 1.431 kHz, 5.507 kHz, 13.437 kHz, 85.948 kHz, 0.127 kHz and 17.879 kHz, respectively. The viscoelasticity influence of the sensitive material on the characteristics of SAW sensors is also studied. By taking account of the viscoelasticity of the PIB layers, the sensitivities of the SAW sensors with the PIB film and PIB nanorods decay in different degree. The gas sensing property of the Love wave sensor with PIB nanorods is superior to that of the PIB films. Meanwhile, the Love wave sensors with PIB sensitive layers show good selectivity to $C_2Cl_4$, making it an ideal selection for gas sensing applications.

**Keywords:** gas sensor, coupled resonance, nano-structure, Love wave

**PACS:** 07.07.Df, 68.35.Iv, 77.65.Dq **DOI:** 10.1088/1674-1056/ac3ec9

## 1. Introduction

Volatile organic compounds (VOCs) have low boiling point and are easy to volatilize at room temperature.[1] VOCs are important precursors of the secondary pollutants, such as fine particulate matter (PM2.5) and ozone ($O_3$). It is well known that the secondary pollutants can cause atmospheric environmental problems, such as haze and photochemical smog.[2,3] Meanwhile, total VOC will do harm to human health, e.g., stimulating human eyes and respiratory tract, causing skin allergy, headache, sore throat and fatigue.[4–6]

In order to protect the environment and human health, real-time, fast and accurate detection of VOCs is particularly important. In recent decades, various types of VOCs sensors have been fabricated, such as the sensors based on resistive, thermo-conductive, electrochemical, and optical technologies.[7] Among them, the conductometric gas sensors based on metal oxides are the remarkable ones for monitoring harmful VOCs, due to the advantages of high sensitivity, portability, rapid response time, real-time detection and low power consumption. However, most of them operate at elevated temperatures (150–500 °C).[8,9] Inevitably, the sensor systems become more complex for requiring heaters, furthermore, the existence of the heater increases the risks of fire and explosion because most of VOCs are inflammable and explosive. Therefore, the design and manufacture of gas sensors operated at room temperature become urgent.

Since 1970s, chemical sensors based on surface acoustic wave (SAW) technology have received more and more attention,[10] due to the characteristics of fast response, low cost, small size, ability to work in wired and wireless mode and so on. These sensors meet the growing demands of high performance sensors in environmental monitoring, industrial production, food hygiene and public health.[11] SAW sensors based on various modes, such as Love wave, Rayleigh wave and Lamb wave,[12] have been fabricated and gained extensive applications. Among them, the Love wave is an effective means to improve the sensing performance, because most of the energy density of which is confined to the guiding layer, and this makes the devices highly sensitive to any perturbation of the surface.

The theoretical and experimental investigations of SAW sensors are continuing reported. Yang *et al.*[13] found that the equivalent circuit model (ECM) is satisfactory in simulating the impedance characteristics of the thickness-shear mode (TSM) sensor in the liquid phase under most conditions except for total immersion of the sensor in highly viscous or conductive liquids. Prior to fabrication of the 300 MHz SAW gas sensor, Wang *et al.*[14] simulated the performances of the sensor by coupling of modes (COM) method. The measured frequency response $S_{12}$ showed a good agreement with simulated results. A P-matrix with new expression derived utilizing the COM theory is used to analyze the tire pressure

†Corresponding author. E-mail: ywang@njupt.edu.cn

© 2022 Chinese Physical Society and IOP Publishing Ltd 

monitoring system (TPMS).[15] The analysis of insertion loss (IL) of the novel SAW sensor based on the new P-matrix model revealed that this design had excellent performance after the parametric optimization. Trivedi *et al.*[16] presented the 3D finite element simulation and analysis of Love wave resonator with different guiding layer materials and investigation of high mass sensitivity caused by the coupled resonance effect with ZnO nanorods on the device surface. On the other hand, Love wave devices have been experimentally demonstrated as sensors for the detection of humidity,[11] gas,[17,18] organic compounds,[19] bacteria,[20] viruses,[21] proteins and immunoglobulins.[22,23]

ECM, COM method and PMM are technologies in common used to simulate the performances of SAW devices. All models need appropriate parameters to describe the physical characteristics of propagation, reflection and transduction of SAWs with respect to different substrates and metallizations.[24] In the analysis of the SAW characteristics, multiple effects affect each other. And even if the individual effects are known with sufficient accuracy, the difference will not yield reliable results.[25] Finite element method (FEM)[24] needs more calculation time and larger running memory, nevertheless, all effects are included. Generally, an eigenvalue problem is solved leading to two eigen-frequencies per propagating mode. From these eigen-frequencies, all relevant parameters and functions can be deduced with exception of the static capacitance.[24]

In this paper, the performances of Love wave devices based on $SiO_2$/ST-90°X quartz structure are analyzed by using FEM. For characterizing the gas sensing properties, polyisobutylene (PIB) is used as the sensitive material due to the great affinity to VOC gases.[26] In addition, the coupled resonance effect induced by PIB nanorods on the improvement of sensitivity is also investigated.

## 2. Theoretical details

The 3D-FEM based on COMSOL multiphysics software is used for the simulation of Love wave devices composed of PIB layers/$SiO_2$/ST-90°X quartz substrate. The Love wave devices can be regarded as infinitely extended periodic structures, and one unit cell is shown in Fig. 1. The four lateral sides of the unit cell are periodic conditions, and the bottom surface is fixed.[27] To excite the SAWs, the interdigital transducers (IDTs), with the same electrodes and period ($\lambda$) of 8 μm, are designed between the $SiO_2$ layer and ST-90°X quartz substrate. The IDTs are set as massless planes in the simulation, and the influence of which on acoustic wave is neglected. As shown in Fig. 1(a), the thicknesses of PIB film, $SiO_2$ guiding layer and ST-90°X quartz substrate are $h_p$, $h_s$ and $4\lambda$, respectively. Meanwhile, as illustrated in Fig. 1(b), PIB nanorods are made over the Love wave device to study the effect of nano-structures on the acoustic properties. The height of PIB nanorod is $h_{pn}$, and the other parameters of the model are the same as Fig. 1(a). The top view of Fig. 1(b) is shown in Fig. 1(c), and the diameters and center distance of the PIB nanorods are 0.4 μm and 2/3 μm, respectively.

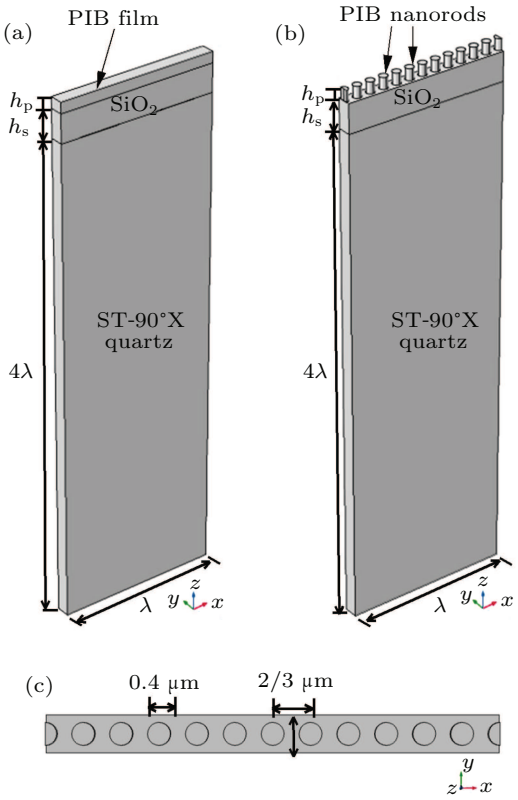



**Fig. 1.** Schematics of the Love wave devices based on $SiO_2$/ST-90°X quartz structure with different PIB layers: (a) PIB films, (b) PIB nanorods; (c) top view of (b).

Resonance frequency $f$, is defined as following:[28]

$$f = (f_s + f_{as})/2, \tag{1}$$

where $f_s$ and $f_{as}$ are the eigen-frequency of symmetric and anti-symmetric mode, respectively.

Mass sensitivity $S_m$ is calculated from the relative frequency shift caused by total mass $\Delta m$ uniformly distributed on the device surface[29]

$$S_m = \frac{\Delta f/f_0}{\Delta m/A}, \tag{2}$$

where $A$ is the area of the device surface, $f_0$ is the resonance frequency of the device without mass loading and $\Delta f = f_0 - f_1$ is the resonance frequency shift due to the mass loading.

The density of sensitive layer can be described as follows:[30]

$$\rho = \rho_0 + \Delta\rho, \tag{3}$$

where $\rho_0$ is the mass density of sensitive layer in air and $\Delta\rho$ is the partial density of the gas molecules adsorbed in the sensitive layer[30]

$$\Delta\rho = K \cdot M \cdot c_0 \cdot \frac{P}{RT}, \tag{4}$$

where $K$ and $M$ are air/PIB partition coefficient and the molar mass of the studied gases, respectively. $c_0$ is the gas concentration in ppm, $P$ and $T$ are the ambient pressure and temperature (1 atm and 25 °C), and $R = 8.3145$ J/(mol·K) is the gas constant. The values of $M$ and $K$ for various VOC gases are shown in Table 1.

Insertion loss (IL) is the attenuation of energy in the process of surface acoustic wave propagation, reflects the energy consumption of SAW device,[31]

$$\mathrm{IL(dB)} = 20\log(|V_{\mathrm{out}}/V_{\mathrm{in}}|), \tag{5}$$

where $V_{\mathrm{in}}$ and $V_{\mathrm{out}}$ are the voltages at the input and output IDT, respectively.

**Table 1.** The values of molar mass $M$ and air/PIB partition coefficient $K$ for various VOC gases.[32]

| Gas | $CH_2Cl_2$ | $CHCl_3$ | $CCl_4$ | $C_2Cl_4$ | $CH_3Cl$ | $C_2HCl_3$ |
|---|---|---|---|---|---|---|
| $M$ (g/mol) | 84.93 | 119.38 | 153.8 | 165.8 | 50.4 | 131.4 |
| $K$ | $10^{1.4821}$ | $10^{1.9273}$ | $10^{2.2060}$ | $10^{2.9799}$ | $10^{0.5538}$ | $10^{2.3994}$ |

## 3. Results and discussion

### 3.1. Admittance of SAW devices

The typical admittance responses of SAW devices based on PIB layers/$SiO_2$/IDT/ST-90°X quartz substrate are shown in Fig. 2(a), in which the thicknesses of $SiO_2$, PIB film and PIB nanorods are 1.4 μm, 0.5 μm and 0.3 μm, respectively. According to the displacements shown in Fig. 2(a), it can be determined precisely that the excited SAW are Love modes for all devices. Figure 2(b) is the admittance curve of Love wave devices with PIB nanorods/$SiO_2$/IDT/ST-90°X quartz substrate structure, in which $h_{\mathrm{pn}}$ is 520 nm. It indicates that the Love waves of mode 0 and mode 1 coexist, and the operating frequencies are $f_0 = 505.8$ MHz and $f_1 = 587.6$ MHz, respectively. As shown in Fig. 2(c), the similar phenomenon is also found for the Love wave device with $h_{\mathrm{pn}}$ of 1260 nm, that is, mode 1 and mode 2 of Love waves coexist.

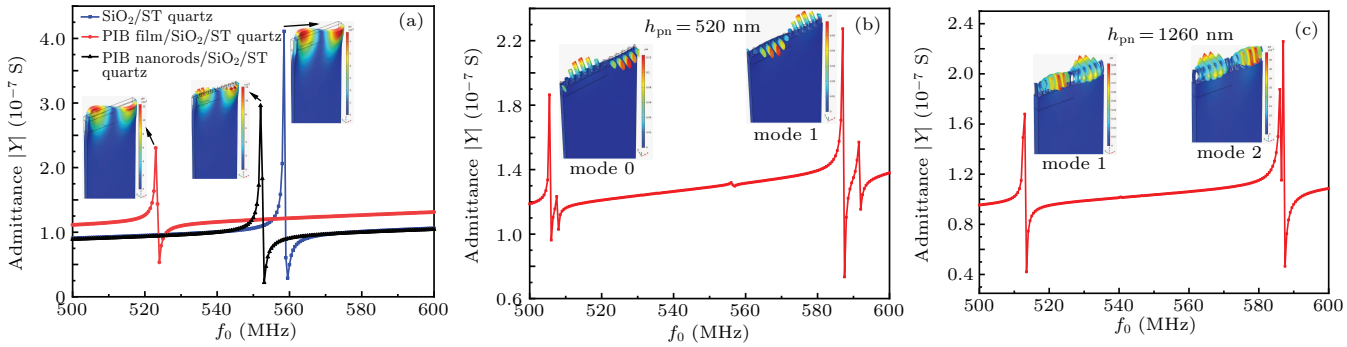



**Fig. 2.** Plots of admittance for SAW devices based on $SiO_2$/ST-90°X quartz structure: (a) with PIB layers; (b)–(c) with PIB nanorods.

### 3.2. Insertion loss

The insertion loss (IL) of the Love wave devices with PIB layers/$SiO_2$/IDT/ST-90°X quartz substrate structure are calculated by using the models shown in Fig. 3, in which the thickness of $SiO_2$, PIB film and PIB nanorods are 1.4 μm, 0.5 μm and 0.52 μm, respectively. Two sides of the model in $x$–$z$ plane are set as periodic boundary conditions, and the other two sides and bottom surface are set as low reflection boundary conditions. A square wave signal with a length of 1 ns and a signal amplitude of 1 V is applied at the input IDT, and then the voltage at the output IDT is received by the probe. Finally, the time-domain voltage data is converted into amplitude frequency characteristics by using FFT, and the IL of the device can be obtained by Eq. (5). The IL of Love wave devices are plotted in Fig. 4. The operating frequencies are 559.32 MHz, 533.16 MHz and 566.48 MHz, respectively, and the corresponding insertion losses are −63.86 dB, −64.36 dB and −64.60 dB, respectively. It can be seen numerically that the attenuations of the Love wave devices increased slightly by the introductions of PIB layers.

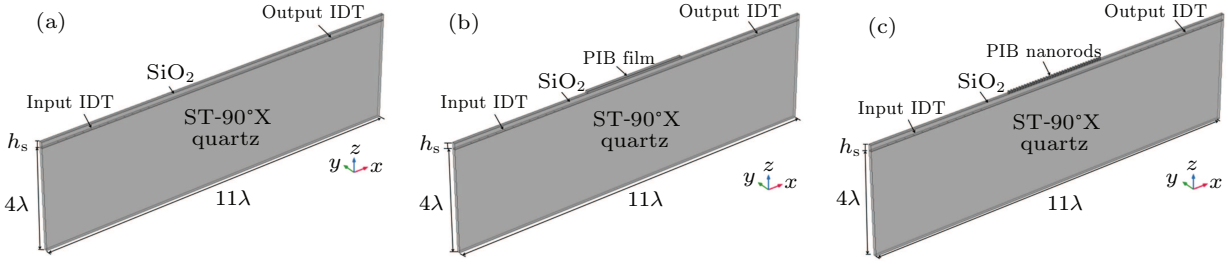



**Fig. 3.** Schematics of Love wave devices based on PIB layers/$SiO_2$/ST-90°X quartz structure: (a) without PIB; (b) with PIB film; (c) with PIB nanorods.

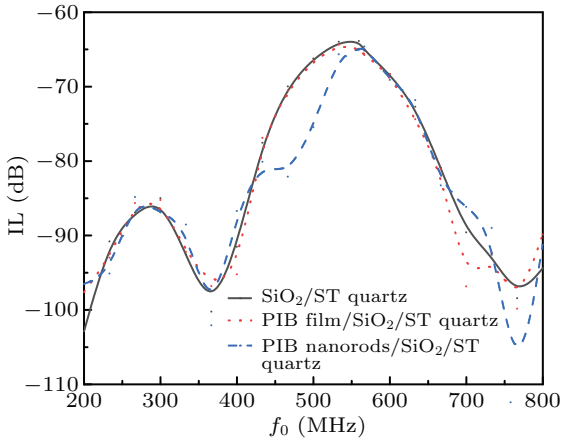



**Fig. 4.** Plots of insertion loss for the Love wave devices based on PIB layers/$SiO_2$/ST-90°X quartz structure.

### 3.3. Resonance frequency

The frequency responses of Love wave devices with PIB layers/$SiO_2$/IDT/ST-90°X quartz substrate structure as functions of the thickness of PIB layers are shown in Fig. 5, in which $h_s$ is set as 1.4 μm. As illustrated in Fig. 5, due to the mass loading and much smaller phase velocity of PIB film,[33] the resonant frequency of PIB film based Love wave device decreases quickly with $h_p$ increasing. On the other hand, for the Love wave device with PIB nanorods, the vibration modes are significantly changed, which agrees well with the results of admittance mentioned above. At a critical height of nanorods, both $SiO_2$/ST-90°X quartz substrate and PIB nanorods vibrate in unison causing a transition from inertial loading to elastic loading and leading to a sharp swing in frequency shift, that is, the coupled resonance.[16] In our case, the first two mode transitions occur at the PIB nanorods height of 500 nm, and 1220 nm, respectively, and the frequency shifts caused by the coupled resonance are 66.22 MHz and 68.38 MHz, respectively. And the typical vibration displacements of mode 0, mode 1 and mode 2 of Love wave are also presented in Fig. 5.

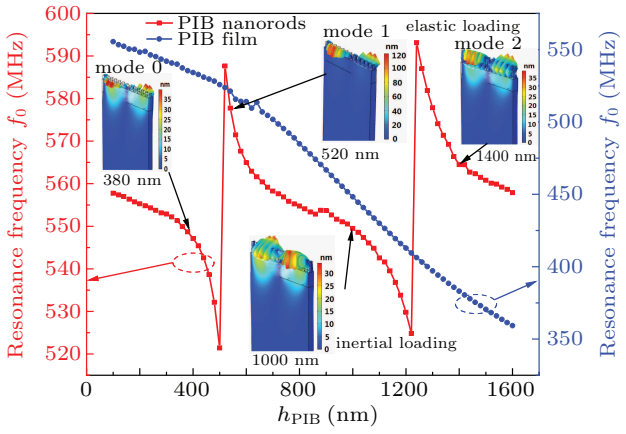



**Fig. 5.** Plots of variations in resonance frequency $f_0$ of Love wave devices with PIB layers/$SiO_2$/IDT/ST-90°X quartz substrate.

The stress ($\sigma$) in $z$ direction of the Love wave devices is calculated and the magnitude of stress for varying thickness of PIB layers is shown in Fig. 6. The stress of the device with PIB film fluctuates around 100 MPa. While, for the devices with PIB nanorods, the stress is about 100 MPa as the absence of coupled resonance, and it reaches nearly 3000 MPa in the presence of coupled resonance at $h_{pn} = 500$ nm and 1220 nm.

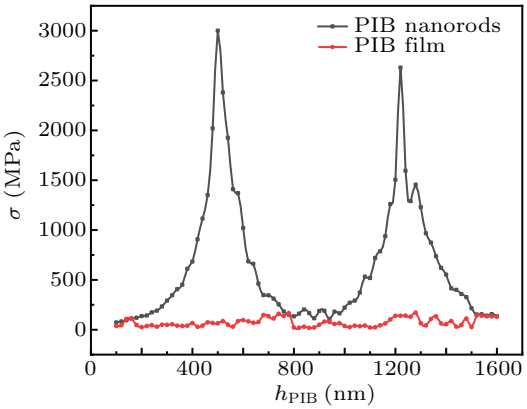



**Fig. 6.** Plots of stress in $z$ direction of Love wave devices with PIB layers/$SiO_2$/IDT/ST-90°X quartz substrate.

### 3.4. Mass sensitivity

The "added mass" feature of COMSOL is used to simulate the mass loading, by which the total mass $\Delta m = 2.448 \times 10^{-15}$ kg is applied on the Love wave sensor with a surface area of $A = 5.33 \times 10^{-12}$ m$^2$ (8 μm×2/3 μm). The mass sensitivity of the Love wave sensors based on PIB layers/$SiO_2$/ST-90°X quartz substrate is shown in Fig. 7.

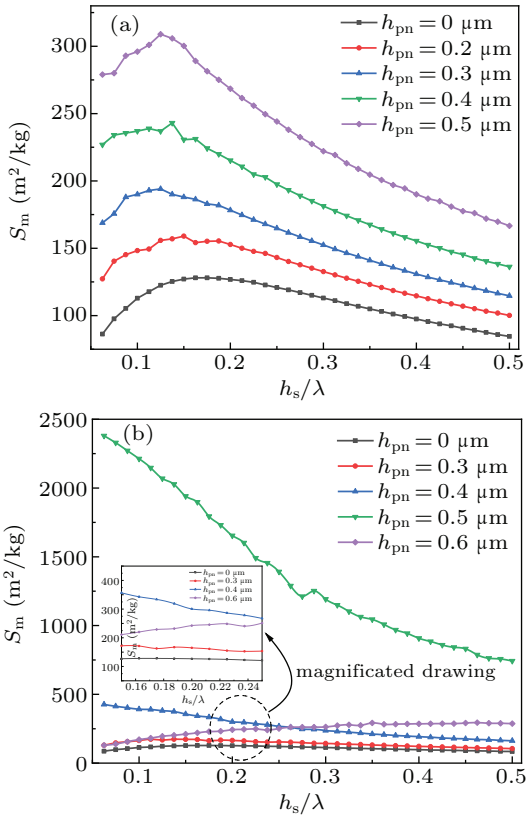



**Fig. 7.** Plots of $S_m$ of Love wave devices based on PIB layers/$SiO_2$/ST-90°X quartz structure as functions of $h_s/\lambda$: (a) PIB film; (b) PIB nanorods.

It can be seen from Fig. 7(a), for the Love wave sensor with structure of $SiO_2$/ST-90°X quartz substrate, that is $h_p = 0$, $S_m$ increases firstly and then decreases with the increase ratio of thickness to wavelength ($h_s/\lambda$), and the maximum value of 128 $m^2$/kg is obtained as $h_s/\lambda$ equaling to 0.175. Meanwhile, the introduction of PIB sensitive film improves $S_m$ of the sensors, and without changing their variation trend with $h_s/\lambda$. The similar tendencies are also found for the Love wave sensors with PIB nanorods as the absence of coupled resonance. However, $S_m$ is improved greatly by the coupled resonance occurred as $h_{pn} = 500$ nm.

### 3.5. Gas sensing property

It is well known that the viscoelasticity of sensitive materials strongly affects the propagation of SAWs. So, it is necessary to study the influences of viscoelastic properties on characteristics of SAW gas sensors for the mechanical loss estimation of the systems. In our calculations, the acoustic velocity of PIB is defined to be complex quantities if the material is viscoelastic, and the parameters used for the simulation are listed in Table 2.

**Table 2.** The viscoelastic parameters of PIB sensitive layers used for simulation in SAW gas sensors.

| Density $\rho$ (kg/m$^3$) | Longitudinal wave velocity $c_p$ (m/s) | Shear wave velocity $c_s$ (m/s) |
|---|---|---|
| 918 | 9781.816+978.1816i | 1918.370+191.8370i |

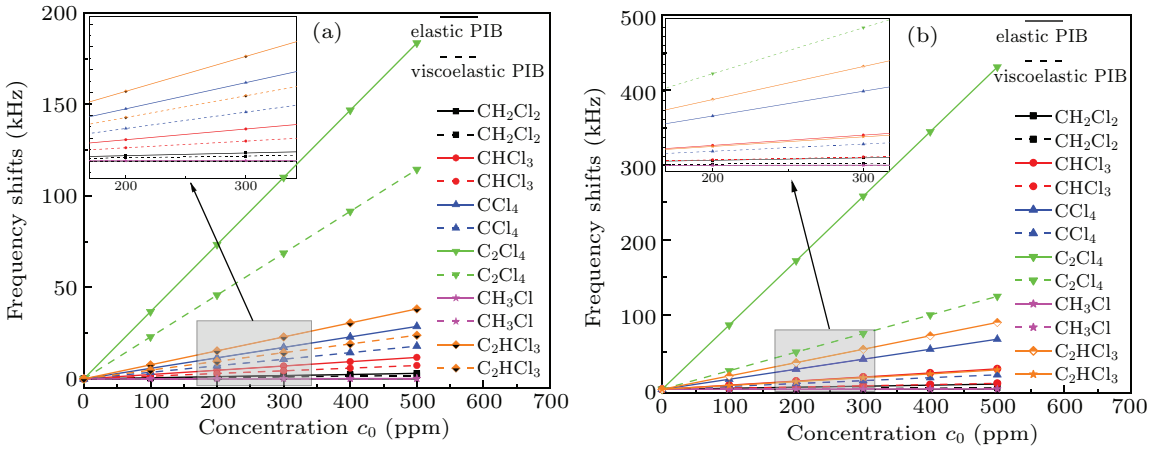



**Fig. 8.** Dynamic response of Love wave sensor based on PIB layers/$SiO_2$/ST-90°X quartz structure towards six VOC gases: (a) PIB film; (b) PIB nanorods.

The Love wave sensors based on PIB layers/$SiO_2$/ST-90°X quartz structure are used for detecting six VOC gases: $CH_2Cl_2$, $CHCl_3$, $CCl_4$, $C_2Cl_4$, $CH_3Cl$ and $C_2HCl_3$, and in which $h_s$ and $h_p$ are 1.4 μm and 0.5 μm, respectively. The frequency shifts $\Delta f$ of Love wave sensors as a function of gas concentration $c_0$ are shown in Fig. 8. Figure 8(a) is the dynamic responses of Love wave sensor with elastic PIB film. It can be seen that, for six VOC gases, the frequency shift $\Delta f$ varies linearly with gas concentration $c_0$ in a wide range from 100 ppm to 500 ppm. Meanwhile, as shown in Fig. 8(b), the frequency shift $\Delta f$ of the Love wave sensor with elastic PIB nanorods varies linearly with the increasing of VOC gas concentration. However, the frequency shifts are approximately 2 times of that of the Love wave sensor with elastic PIB film. As $c_0 = 100$ ppm, the frequency shifts of the sensors corresponding to $CH_2Cl_2$, $CHCl_3$, $CCl_4$, $C_2Cl_4$, $CH_3Cl$ and $C_2HCl_3$ are 1.431 kHz, 5.507 kHz, 13.437 kHz, 85.948 kHz, 0.127 kHz and 17.879 kHz, respectively. In addition, compared with elastic PIB layers, the sensitivity of SAW sensors with viscoelastic PIB film and PIB nanorods decay in different degree and attenuate by approximately 40% and 70%, respectively. Although the viscoelasticity of PIB sensitive material has a greater impact on the sensor with PIB nanorods/$SiO_2$/ST-90°X quartz structure, but the sensitivity of which is still superior to that with PIB film structure. The frequency shifts of SAW sensors with PIB layers/$SiO_2$/ST-90°X quartz structures to VOC gases with the concentration of 100 ppm are listed in Table 3.

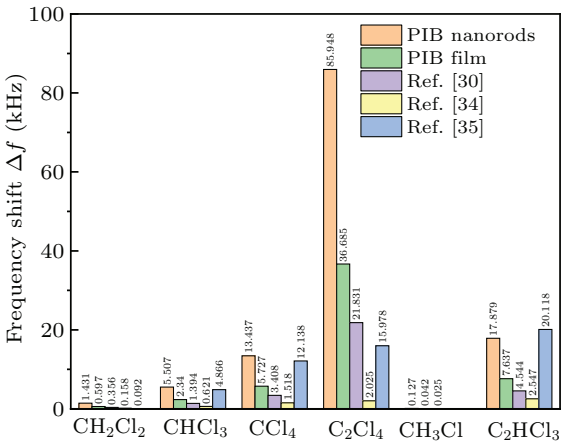



**Fig. 9.** Frequency shifts of five sensors exposed to 100 ppm of different VOC gases.

**Table 3.** The frequency shifts of various sensors exposed to 100 ppm of six VOC gases.

| Sensors | $\Delta f$ (kHz) | | | | | |
|---|---|---|---|---|---|---|
| | $CH_2Cl_2$ | $CHCl_3$ | $CCl_4$ | $C_2Cl_4$ | $CH_3Cl$ | $C_2HCl_3$ |
| Elastic PIB nanorods/$SiO_2$/ST-90°X quartz | 1.431 | 5.507 | 13.437 | 85.948 | 0.127 | 17.879 |
| Viscoelastic PIB nanorods/$SiO_2$/ST-90°X quartz | 0.446 | 1.627 | 3.925 | 24.879 | 0.029 | 5.180 |
| Elastic PIB films/$SiO_2$/ST-90°X quartz | 0.597 | 2.340 | 5.727 | 36.685 | 0.042 | 7.637 |
| Viscoelastic PIB films/$SiO_2$/ST-90°X quartz | 0.373 | 1.460 | 3.574 | 22.891 | 0.026 | 4.766 |
| Elastic PIB thin film/YZ-$LiNbO_3$ [30] | 0.356 | 1.394 | 3.408 | 21.831 | 0.025 | 4.544 |
| Elastic PIB thin film/AlN/Si [34] | 0.158 | 0.621 | 1.518 | 2.025 | – | 2.547 |
| GO/$SiO_2$/128°YX-$LiNbO_3$ [35] | 0.092 | 4.866 | 12.138 | 15.978 | – | 20.118 |

The sensitivities of different sensors for detecting VOC gases with the concentration of 100 ppm are indicated in Fig. 9, and the exact values are listed in Table 3. Obviously, the Love wave sensor with elastic PIB nanorods has superior sensing performances to the others, and shows good selectivity to $C_2Cl_4$, making it a highly sensitive sensing platform.

## 4. Conclusion

The properties of Love wave sensors based on $SiO_2$/ST-90°X quartz structure are simulated by 3D-FEM, in which PIB films and PIB nanorods are used as sensing layers, respectively. The mass sensitivity of the basic Love wave device with $SiO_2$ guiding layer of varying thickness is solved analytically. And the highest mass sensitivity of 128 $m^2$/kg is obtained as $h_s/\lambda = 0.175$. In addition, the effects of nanorods with different heights on the mass sensitivity are also investigated. The Love wave sensors with PIB sensitive layers are used for the detection of six VOC gases, and the results indicate that the presence of PIB nanorods causes coupled resonance, resulting in an enhanced gas sensitivity of the device. The frequency shifts of the sensor corresponding to $CH_2Cl_2$, $CHCl_3$, $CCl_4$, $C_2Cl_4$, $CH_3Cl$ and $C_2HCl_3$ are 1.431 kHz, 5.507 kHz, 13.437 kHz, 85.948 kHz, 0.127 kHz and 17.879 kHz, respectively. The gas sensing properties of Love wave sensor are greatly improved by PIB nanorods than that of the PIB films based sensor. However, the sensitivities of SAW sensors with the viscoelastic PIB film and viscoelastic PIB nanorods decay in different degree and decline by about 40% and 70%, respectively. Meanwhile, the Love wave sensors with PIB sensitive layers show good selectivity to $C_2Cl_4$, making it a highly sensitive sensing platform.

## Acknowledgement

Project supported by the Foundation of Nanjing University of Posts and Telecommunications, China (Grant No. NY213018).

## References

[1] Wang H L, Nie L, Li J, Wang Y F, Wang G, Wang J H and Hao Z P 2013 *Chin. Sci. Bull.* **58** 724
[2] Geng F H, Tie X X, Xu J M, Zhou G Q, Peng L, Gao W, Tang X and Zhao C S 2008 *Atmos. Environ.* **42** 6873
[3] Shao M, Zhang Y H, Zeng L M, Tang X Y, Zhang J, Zhong L J and Wang B G 2009 *J. Environ. Manage.* **90** 512
[4] Mirzaei A, Leonardi S G and Neri G 2016 *Ceram. Int.* **42** 15119
[5] Hempel-Jorgensen A, Kjaergaard S K, Molhave L and Hudnell K H 1999 *Arch. Environ. Health* **54** 416
[6] Pawar D, Kanawade R, Kumar A, Rao C N, Cao P J, Gaware S, Late D, Kale S N, Navale S T, Liu W J, Zhu D L, Lu Y M and Sinha R K 2020 *Sens. Actuator B-Chem.* **312** 127921
[7] Kumar P, Deep A, Kim K and Brown R J C 2015 *Prog. Polym. Sci.* **45** 102
[8] Lu F, Liu Y, Dong M and Wang X P 2000 *Sens. Actuator B-Chem.* **66** 225
[9] Huang J R, Wu Y J, Gu C P, Zhai M H, Sun Y F and Liu J H 2011 *Sens. Actuator B-Chem.* **155** 126
[10] Devkota J, Ohodnicki P R and Greve D W 2017 *Sensors* **17** 801
[11] Gronewold T M A 2007 *Anal. Chim. Acta* **603** 119
[12] Wohltjen H 1984 *Sens. Actuator* **5** 307
[13] Yang M S and Thompson M 1993 *Analytica Chimica Acta* **282** 505
[14] Wang W, He S T, Li S Z, Liu M H and Pan Y 2007 *Sens. Actuator B-Chem.* **125** 422
[15] Zheng L, Liu T, Hu H and Li T L 2008 *3rd IEEE International Conference on Nano/Micro Engineered and Molecular Systems*, Janusry 6–9, 2008, Sanya, China, p. 462
[16] Trivedi S and Nemade H B 2018 *Ultrasonics* **84** 150
[17] Jakoby B, Ismail G M, Byfield M P and Vellekoop M J 1999 *Sens. Actuator A-Phys.* **76** 93
[18] Youssef I B, Alem H, Sarry F, Elmazria O, Rioboo R J and Arnal-Hérault 2013 *Sens. Actuator B-Chem.* **185** 309
[19] Zimmermann C, Rebière D, Déjous C, Pistré J, Chastaing E and Planade R 2001 *Sens. Actuator B-Chem.* **76** 86
[20] Branch D W and Brozik S M 2004 *Biosens.Bioelectron.* **19** 849
[21] Zhang X, Fang J R, Zou L, Zou Y C, Lang L, Gao F, Hu N and Wang P 2016 *Biosens. Bioelectron.* **77** 573
[22] Zou L, Tian Y L, Zhang X, Fang J R, Hu N and Wang P 2017 *Sens. Actuator B-Chem.* **238** 1173
[23] Gizeli E, Bender F, Rasmusson A, Saha K, Josse F and Cernosek R 2003 *Biosens. Bioelectron.* **18** 1399
[24] Ruppel C C W, Ruile W, Scholl G, Wagner K C and Manner O 1994 *Ultrasonics Symposium*, October 31–November 3, 1994, Cannes, France, p. 413
[25] Robinson H, Hahn Y and Gau J N 1989 *J. Appl. Phys.* **65** 4573
[26] Aslam M Z, Jeoti V, Karuppanan S, Malik A F and Iqbal A 2018 *Sensors* **18** 1687
[27] Trivedi S and Nemade H B 2018 *Microsyst. Technol.* **24** 3537
[28] Plessky V and Koskela J 2000 *Int. J. High Speed Electron. Syst.* **10** 867

[29] Du J, Harding G L, Ogilvy J A, Dencher P R and Lake M 1996 *Sens. Actuator A-Phys.* **56** 211

[30] Johnson S and Shanmugananthan D T 2014 *Int. Journal of Engineering Research and Applications* **4** 254

[31] Huang I Y, Lin C Y and Lan J W 2013 *J. Micro/Nanolithogr., MEMS, MOEMS* **12** 013019

[32] Ho C K, Lindgren E R, Rawlinson K S, Mcgrath L K and Wright J L 2003 *Sensors* **3** 236

[33] Greate J W and Patrash S J 1995 *Anal. Chem.* **67** 2162

[34] Caliendo C and Hamidullah M 2017 *J. Phys. D-Appl. Phys.* **50** 474002

[35] Xu X 2019 *Study on the characteristics of surface acoustic wave devices based on graphene oxide films* (MS Thesis) (Nanjing: Nanjing University of Posts and Telecommunications) (in Chinese)